Open access • Journal Article • DOI:10.1103/PHYSREVA.40.2417

Quantum dynamics of the nonlinear rotator and the effects of continual spin measurement. — Source link

Barry C. Sanders

Institutions: University of Queensland

Published on: 01 Sep 1989 - Physical Review A (American Physical Society)

Topics: Open quantum system, Quantum dynamics, Quantum technology, Quantum algorithm and Quantum error correction

Quantum dynamics of the nonlinear rotator and the effects of continual spin measurement

Barry C. Sanders
Department of Physics, University of Queensland, Saint Lucia, Queensland, Australia 4067
(Received 17 April 1989)

The quantum and classical dynamics of the nonlinear oscillator are contrasted by comparing the evolution of the quantum Q function with that of a similar classical probability distribution. The quantum nonlinear rotator is shown to generate a superposition of two distinct coherent states from a coherent-state input. Measurements of the angular-momentum components and the signature of a superposition state are discussed. The effects of a continual measurement of one angular-momentum component are introduced into the model, and its effects on quantum coherences are shown to degrade the quantum coherence effects. We present a quantum optical model that obeys the nonlinear rotator dynamics and can generate superpositions of SU(2) coherent states of the two-mode electromagnetic field.

I. INTRODUCTION

The quantum nonlinear oscillator possesses important features which have led to vigorous interest in the model,[1-7] and the nonlinear rotator, which is investigated here, is demonstrated to share many important properties. The exactly solvable dynamics of the nonlinear oscillator has led to a revealing investigation of the classical and quantum dynamics by comparing the joint phase-space probability density evolutions for the two regimes.[1-3] The classical distribution in phase space undergoes a rotational shear, which leads to a fine-scale convolution of the original distribution. The quantum probability density is prevented from developing a fine-scale structure by the presence of second-order terms in the differential equation. Instead, quantum coherences cause the dynamics of the nonlinear oscillator to be periodic.[1-4,6,7] Furthermore, the quantum nonlinear oscillator transforms an initial coherent state into a superposition of two coherent states which are separated by a phase of π.[3,4,6,7] The detection of such superposition states can be performed via quadrature-phase measurements: the in-phase quadrature-phase eigenvalue distribution is double peaked and the out-of-phase quadrature distribution displays interference fringes.[3,4,6,7]

The nonlinear rotator is a spin system which is subjected to a quadratic precession about one axis. The nonlinear oscillator and the nonlinear rotator appear very different. The Heisenberg-Weyl group is the symmetry group for the nonlinear oscillator, whereas SU(2) is the symmetry group for spin precession. Moreover, physical examples of the nonlinear oscillator, such as for the self-interaction of the electromagnetic field,[5] are quite different from realizations of spin precession in, say, a nuclear system.[8] Nevertheless, there exist many common features between the systems, as we shall observe.

The comparison of the classical and quantum dynamics of the nonlinear rotator is performed in Sec. II by studying the evolution of a probability density for the system. For the quantum nonlinear oscillator the Q-function description is employed as it is a true probability density, and each quantum state is completely determined by the Q function.[9] Similarly, the density matrix of the nonlinear rotator is completely determined by the Q function corresponding to the SU(2) group[10] and we compare the classical and quantum dynamics by contrasting an evolving classical probability distribution with a time-dependent quantum Q function. We also study the eigenvalue distributions of the angular-momentum operators for the evolving state and determine the signatures of quantum coherences.

Continuous measurement is included in the model in Sec. III. Measurements of an angular-momentum component occur by coupling a meter to the component being measured.[11-14] The meter is quantized and the quantum fluctuations feed back into the measured nonlinear rotator, but the measurement scheme is nondissipative. Continuous measurement of one component of angular momentum introduces fluctuations into the other components. The effects of continuous measurement on the quantum coherences of the nonlinear rotator are determined.

Several possibilities for realizing the nonlinear rotator exist. The quadratic precession arises for the interaction of a nucleus interacting with an axially symmetric field[8] or for an anisotropic crystal in a magnetic field.[15] A third possibility exists for the two-mode field interaction which is discussed in detail in Sec. IV. In this quantum optical model the nonlinear rotator dynamics discussed here can, in principle, be tested.

II. CLASSICAL AND QUANTUM DYNAMICS

The Hamiltonian for the nonlinear rotator is

$$H_j=\omega J_z+\frac{\lambda}{2j}J_z^2\ , \tag{2.1}$$

where ω is the linear precession frequency and λ is a positive constant. The classical dynamics are described by the motion of the angular-momentum vector $\mathbf{J}$ through three-dimensional space and $|\mathbf{J}|=j$ is a constant. The initial conditions for the classical nonlinear rotator is

specified as a probability distribution of vectors **J** which we assume to be of equal magnitude j. Thus, the distribution of vectors can be represented as a distribution of points on the sphere of radius j and the parametrization

$$\mathbf{J}/j=(\sin\theta\cos\phi,\sin\theta\sin\phi,\cos\theta) \tag{2.2}$$

is used. Alternatively, the stereographic projection of the sphere onto the complex plane is useful. The stereographic map is given by

$$\gamma=e^{i\phi}\tan(\theta/2)\ . \tag{2.3}$$

The north pole ($J_z=j$) is mapped to the origin ($\gamma=0$) and the south pole is mapped to infinity. The equator is mapped to the unit circle. The stereographic map is conformal and, moreover, maps circles to circles or to axial lines. Thus, a distribution with circular contours is generally mapped to a distribution with circular contours.

The distribution of vectors **J** is given by a distribution $Q_j(\gamma)$ over the complex plane. The equations of motion for the components of **J** are obtained from (2.1) by employing the Poisson-bracket relations $[J_i,J_j]_P=\sum_k\epsilon_{ijk}J_k$ and $dJ_i/dt=-[H,J_i]_P$. Thus the equation of motion for γ is

$$\frac{d\gamma}{dt}=i\left[\omega+\lambda\frac{1-|\gamma|^2}{1+|\gamma|^2}\right]\gamma\ . \tag{2.4}$$

As

$$\frac{J_z}{j}=\frac{1-|\gamma|^2}{1+|\gamma|^2} \tag{2.5}$$

is a constant of motion, so is $|\gamma|^2$, and Eq. (2.4) is readily integrated to produce

$$\gamma(t)=\exp\left[-i\left[\omega+\lambda\frac{1-|\gamma|^2}{1+|\gamma|^2}\right]t\right]\gamma(0)\ . \tag{2.6}$$

The first-order differential equation for the time-dependent distribution $Q_j(\gamma;t)$ is, therefore,

$$\frac{\partial}{\partial t}Q_j(\gamma;t)=-i\left[\omega+\lambda\frac{1-|\gamma|^2}{1+|\gamma|^2}\right]\gamma\frac{\partial}{\partial\gamma}Q_j(\gamma;t)+\text{c.c.}\ , \tag{2.7}$$

where c.c. refers to the complex conjugate. The distribution thus undergoes a linear rotation at the frequency ω and a shear proportional to J_z/j occurs in the stereographic plane. The choice of the nonlinear coefficient $\lambda/2j$ in (2.1) ensures that the shearing rate is j independent in (2.7). An initial point in the complex plane γ is mapped to itself at the time

$$t=2\pi[\omega+\lambda(1-|\gamma|^2)/(1+|\gamma|^2)]^{-1}$$

which is independent of j.

The Hamiltonian for the quantum model is given by (2.1) for $\hbar=1$ and **J** is the angular-momentum operator which satisfies the commutation relation $\mathbf{J}\times\mathbf{J}=i\mathbf{J}$, that is, the algebra of the SU(2) group. The scalar operator $\mathbf{J}\cdot\mathbf{J}$ is a constant of motion with eigenvalue $j(j+1)$ for j henceforth assumed to be an integer. An orthonormal basis for the Hilbert space can be constructed from the $2j+1$ eigenstates of the angular-momentum component operator

$$J_{\mathbf{n}}\equiv\mathbf{J}\cdot\mathbf{n} \tag{2.8}$$

for **n** a unit vector. The eigenstates of $J_{\mathbf{n}}$, given by $\{|jm\rangle_{\mathbf{n}}\}$ for $-j\le m\le j$, satisfy the eigenvalue equation

$$J_{\mathbf{n}}|jm\rangle_{\mathbf{n}}=m|jm\rangle_{\mathbf{n}}\ . \tag{2.9}$$

The SU(2) coherent states provide an alternate, overcomplete basis for the Hilbert space. For $J_+\equiv J_x+iJ_y=J_-^\dagger$, the unitary rotation operator is given by[10]

$$R(\gamma)=\exp[-\tfrac{1}{2}\theta(J_+e^{-i\varphi}-J_-e^{i\varphi})] \tag{2.10}$$

for γ the complex parameter in Eq. (2.3). The antinormally ordered rotation operator is[10]

$$R(\gamma)=\exp(\gamma J_-)\exp[-J_z\ln(1+|\gamma|^2)]\exp(-\gamma^*J_+)\ . \tag{2.11}$$

Expression (2.9) allows us to compute the matrix elements of the SU(2) coherent state

$$|\gamma\rangle=R(\gamma)|jj\rangle=(1+|\gamma|^2)^{-j}\sum_{m=0}^{2j}\binom{2j}{m}^{1/2}\gamma^m|j\,j-m\rangle\ , \tag{2.12}$$

which is obtained by rotating $|j\,j\rangle$ by the angle θ about the vector $(\sin\phi,-\cos\phi,0)$.

The density operator ρ_j specifies the quantum state, and the corresponding Q function on the stereographic plane is defined by

$$Q_j(\gamma;t)\equiv\langle j\gamma|\rho_j(t)|j\gamma\rangle\ , \tag{2.13}$$

which is a true probability density and completely determines the state $\rho_j(t)$.[8] Taking the coherent-state expectation value of the master equation

$$\frac{\partial}{\partial t}\rho_j=-i[H_j,\rho_j] \tag{2.14}$$

produces the differential equation

$$\frac{\partial}{\partial t}Q_j(\gamma;t)=-i\left[\omega+\lambda\frac{1-|\gamma|^2}{1+|\gamma|^2}-\frac{\lambda}{2j}\gamma\frac{\partial}{\partial\gamma}\right]\times\gamma\frac{\partial}{\partial\gamma}Q_j(\gamma;t)+\text{c.c.} \tag{2.15}$$

In the semiclassical limit $j\to\infty$ and ω and λ are constant. The classical first-order differential equation (2.7) is obtained in the semiclassical limit, as required by the correspondence principle, and is j independent. The second-order differential terms are responsible for differences between the classical and quantum evolution of the probability density $Q_j(\gamma;t)$.[1,2]

The quantum nonlinear rotator is prepared in the SU(2) coherent state $\rho=|j\gamma_0\rangle\langle j\gamma_0|$. Thus the initial Q function for the nonlinear rotator is

$$Q_j(\gamma,0)=\left[\frac{(1+\gamma_0^*\gamma)(1+\gamma_0\gamma^*)}{(1+\gamma_0\gamma_0^*)(1+\gamma\gamma^*)}\right]^{2j}\ . \tag{2.16}$$

The distribution is localized with a peak at γ_0 and the circular contours are nonconcentric. The contour of height h is given by the equation for the circle

$$|\gamma-\gamma_h|=r_h \tag{2.17}$$

for

$$\gamma_h=[1-(1-h^{1/2j})(1+|\gamma_0|^2)]^{-1}\gamma_0 , \tag{2.18}$$

the center, and

$$r_h=\frac{\gamma_h}{\gamma_0}[h^{1/2j}(1-h^{1/2j})(1+|\gamma_0|^2)]^{1/2} , \tag{2.19}$$

the radius. The Q function for $\gamma_0=0.65$ and $j=20$ is shown in Fig. 1(a). Let us assume that the classical rotator is prepared in the state (2.16) and compare the classical and quantum evolutions of the probability density.

The time-dependent classical distribution can be shown to be $Q_j(\gamma;t)=Q_j(\gamma(-t))$ for $Q_j(\gamma,0)$ given by (2.16) and $\gamma(t)$ given by (2.6). The classical distribution for $j=20$, $\gamma_0=0.65$, $\omega=0$, $\lambda=3$, and $t=16\pi/15$ is shown in Fig. 1(b) and a rotational shear is evident. For large t the distribution becomes convoluted about the origin, similar to the classical distribution evolution for the nonlinear oscillator.[1-3]

For the quantum nonlinear rotator, the time-dependent Q function is

$$Q(\gamma;t)=\left|\sum_{m=0}^{2j} S_m^j(\gamma;t)\right|^2 , \tag{2.20}$$

where

$$S_m^j(\gamma;t)\equiv[(1+|\gamma_0|^2)(1+|\gamma|^2)]^{-j}\begin{bmatrix}2j\\m\end{bmatrix} \times\exp\left[-i\frac{\lambda t}{2j}m^2\right](e^{-i\omega t}\gamma\gamma_0^*)^m . \tag{2.21}$$

The Q function (2.18) satisfies the differential equation (2.13) for $Q(\gamma;0)$ given by (2.16), and the Q function for $t=0$ corresponds to that of the initial coherent state $|j\gamma_0\rangle$. The quantum dynamics is evidently periodic with a recurrence time of

$$\tau_j=4\pi j/\lambda . \tag{2.22}$$

For times small compared with τ_j the quantum coherence effects are weak. Thus for small times, the behavior of the quantum Q function and the classical distribution are similar. For longer times, on the order of τ_j, the quantum and classical evolutions of the Q function differ. In the semiclassical limit the period becomes large and thus the break time between classical and quantum behavior also becomes quite long. The proportionality between τ_j and j is a consequence of the scaling of the nonlinear coefficient $\lambda/2j$ in the Hamiltonian (2.1). Alternately the nonlinear coefficient in (2.1) could be independent of j. In this case the recurrence time τ_j would also be independent of j, but the break time between the classical and quantum evolutions of the Q function would scale inversely with j. In Fig. 1(c) the Q function for $t=\tau/25=16\pi/15$ is presented for $j=20$, $\gamma_0=0.65$, $\omega=0$, and $\lambda=3$. Whereas the classical distribution in Fig. 1(b) for $t=16\pi/15$ is sheared and presents a fine-scale convolution structure, the quantum coherences in the Q function, evidenced by the ripples, prevent the convolutions from occurring.

The Q function for $t=\tau_j/4$, shown in Fig. 1(d), has evolved into the superposition state

$$\exp(-H_j\tau_j/4)|j\gamma_0\rangle =2^{-1/2}[e^{-i\pi/4}|j\gamma_0\rangle+(-1)^j e^{i\pi/4}|j-\gamma_0\rangle] . \tag{2.23}$$

A superposition of two distinct coherent states, separated by a phase of π, has been generated from an initial coherent state, analogous to the superposition state of the nonlinear oscillator.[3,4,6,7] However, the phase difference of the coefficients in (2.20) depends on whether j is even or odd. At the later time, $t=\tau_j/2$ the coherent state $(-1)^j|j\ -\gamma_0\rangle$ is generated.

The superposition of two coherent states generated by the nonlinear oscillator is detected via ideal quadrature-phase measurements.[3,6,7] For example, the superposition of the two Glauber coherent states $|\alpha\rangle$ and $|-\alpha\rangle$, for α real, produces a double-peaked distribution for measurements of the in-phase quadrature and the peaks are localized at $\pm\alpha$. The out-of-phase quadrature measurements conform to a distribution with a mean of zero and strong interference fringes are evident. An analogous approach is adopted below to detect the superposition of $|j\gamma_0\rangle$ and $|j-\gamma_0\rangle$.

For a spin system, the components of the angular momentum J_x, J_y, and J_z are measured. Unlike the quadrature-phase spectrum, which is continuous and unbounded, the angular-momentum spectra are discrete and bounded. The eigenvalue distribution of the state ρ_j for the angular-momentum operator component $\mathbf{J}\cdot\mathbf{n}$ is given by ${}_{\mathbf{n}}\langle jm|\rho_j|jm\rangle_{\mathbf{n}}$, $-j\le m\le j$. The statistics of ideal measurements of $\mathbf{J}\cdot\mathbf{n}$ for the state ρ_j conform to the $\mathbf{J}\cdot\mathbf{n}$ eigenvalue distribution. For the coherent state $|j=20,\ \gamma_0=0.65\rangle$, the eigenvalue probability distributions for J_x, J_y, and J_z are shown in Fig. 2. The eigenvalue distributions are localized about $\langle J_x\rangle/j=0.91$, $\langle J_y\rangle/j=0$, and $\langle J_z\rangle/j=0.41$, respectively, which corresponds to the mean of the coherent state $|j=20,\ \gamma_0=0.65\rangle$. In Fig. 3 the J_x and J_y eigenvalue distributions for the superposition state (2.20), where $j=20$ and $\gamma_0=0.65$, are shown. A double-peaked distribution is observed in the J_x distribution and interference fringes are present in the zero-centered J_y distribution. These two distributions characterize a coherent superposition of two SU(2) coherent states.[14] In the J_z basis the distribution for the superposition state is identical to the J_z eigenvalue distribution of $|j\gamma_0\rangle$ shown in Fig. 3(c). The J_z eigenvalue distribution is unchanged because J_z is a constant of motion. The superposition state (2.23) involves coefficients which are separated in phase by $\pi/2$, but a more general superposition of $|j\gamma_0\rangle$ and $|j-\gamma_0\rangle$ for which the coefficients have an arbitrary phase separation, would be expected to produce a J_z eigenvalue distribution different from that of $|j\gamma_0\rangle$.[7]

III. THE EFFECTS OF CONTINUAL SPIN MEASUREMENT

The J_z eigenvalue distribution, which corresponds to the statistics of perfect J_z measurements for the state, is constant over time. In this section we assume that a meter, which continually measures J_z, is coupled to the rotator. A general class of nondissipative continual measurements of J_z is given by the master equation[12–14]

$$\frac{\partial}{\partial t}\rho_j = -i[H_j,\rho_j] - \frac{\Gamma}{2_j}[J_z,[J_z,\rho_j]] \tag{3.1}$$

for H_j the Hamiltonian (2.1). The parameter Γ fixes the resolution of the J_z measurements. The scaling $\Gamma/2j$ is introduced to ensure that the resolution scales linearly with the width of the eigenvalue spectrum.[14] Essentially, measurements of J_z introduce fluctuations into the J_x and J_y components, while J_z remains a constant of motion.

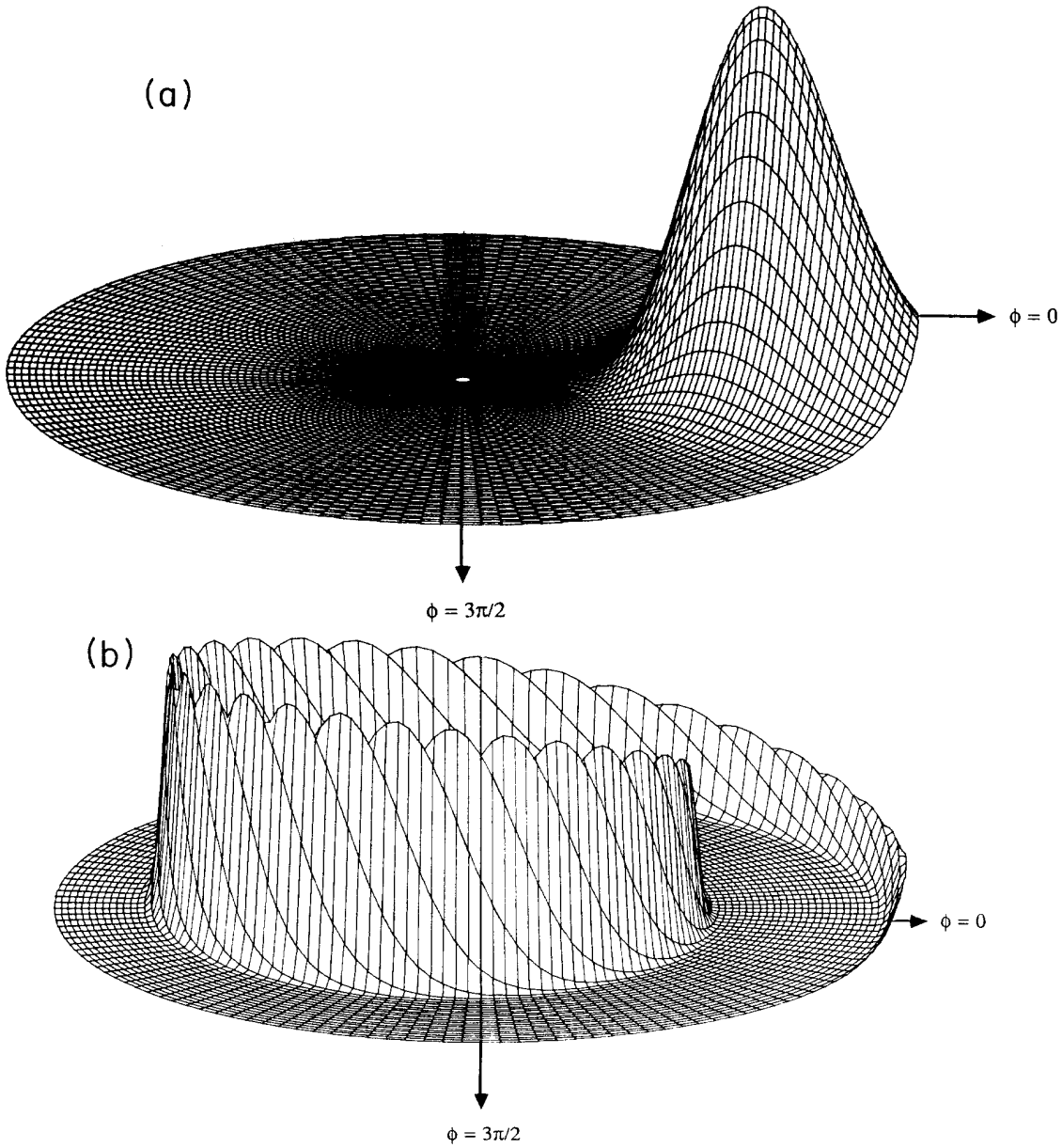

FIG. 1. Polar view of the probability density $Q(\gamma;t)$ on the complex stereographic plane for $j=20$, $\gamma_0=0.65$, $\omega=0$, and $\lambda=3$. For $\gamma=re^{i\phi}$ the domain is restricted to $r\leq 1$ and the phases $\phi=0$ and $\phi=3\pi/2$ are indicated on the graphs. The initial probability density $Q(\gamma;0)$ which is identical for the classical and quantum nonlinear rotators, is shown in (a) and the maximum value is $Q_{\max}=1.00$. The density $Q(\gamma;t=16\pi/15)$ is shown for (b) the classical rotator ($Q_{\max}=1.00$) and (c) the quantum rotator ($Q_{\max}=0.23$). The quantum density $Q(\gamma;t=20\pi/3)$ is shown in (d) where $Q_{\max}=0.50$.

This is seen clearly in the solution of (3.1) in the J_z eigenbasis. For $\rho_{nm}=\langle jn|\rho|jm\rangle$, the density-matrix elements are given by

$$\rho_{nm}(t)=\exp\left[-i\left[\omega(n-m)+\frac{\lambda}{2j}(n^2-m^2)\right]-\frac{\Gamma}{2j}(n-m)^2\right]\rho_{nm}(0)\ . \tag{3.2}$$

Thus strong measurements of J_z destroy the off-diagonal elements in the J_z basis.

The evolution of the Q function in the measured system is obtained by determining the coherent-state expectation value of (3.1). The master equation

$$\frac{\partial}{\partial t}Q_j(\gamma;t)=-i\left[\omega+\lambda\frac{1-|\gamma|^2}{1+|\gamma|^2}-\frac{\lambda}{2j}\gamma\frac{\partial}{\partial\gamma}\right]\times\gamma\frac{\partial}{\partial\gamma}Q_j(\gamma;t)+\text{c.c.}-\frac{\Gamma}{2j}\left[\gamma\frac{\partial}{\partial\gamma}-\gamma^*\frac{\partial}{\partial\gamma^*}\right]^2Q_j(\gamma;t) \tag{3.3}$$

includes the differential terms from Eq. (2.15) and there are second-order differentials which are responsible for the modification of Q due to measurement. The effects of the measurement can be better understood by introducing the polar coordinates r and ϕ such that $\gamma=re^{i\phi}$. Thus the measurement-induced modification in the differential equation (3.3) is given by

$$-\frac{\Gamma}{2j}\left[\gamma\frac{\partial}{\partial\gamma}-\gamma^*\frac{\partial}{\partial\gamma^*}\right]^2Q_j(\gamma)=\frac{\Gamma}{2j}\frac{\partial^2}{\partial\phi^2}Q_j(r,\phi)\ , \tag{3.4}$$

which corresponds to phase diffusion with a diffusion coefficient $\Gamma/2j$. The phase diffusion coefficient $\Gamma/2j$ and the quantum coherence coefficient $\lambda/2j$ both scale inversely with j and become very small in the semiclassical limit. In the semiclassical limit ($j\rightarrow\infty$), the quantum coherences and the phase diffusion terms become very small and the classical equation (2.7) is restored. Equivalently the classical and quantum evolutions of the Q function are similar for short times such that $t\ll 2j/\lambda$ and $t\ll 2j/\Gamma$.

The nonlinear rotator is prepared in the coherent state $|j\gamma_0\rangle$; hence (2.11) serves as the initial condition for (3.3). The solution to (3.3) is given by

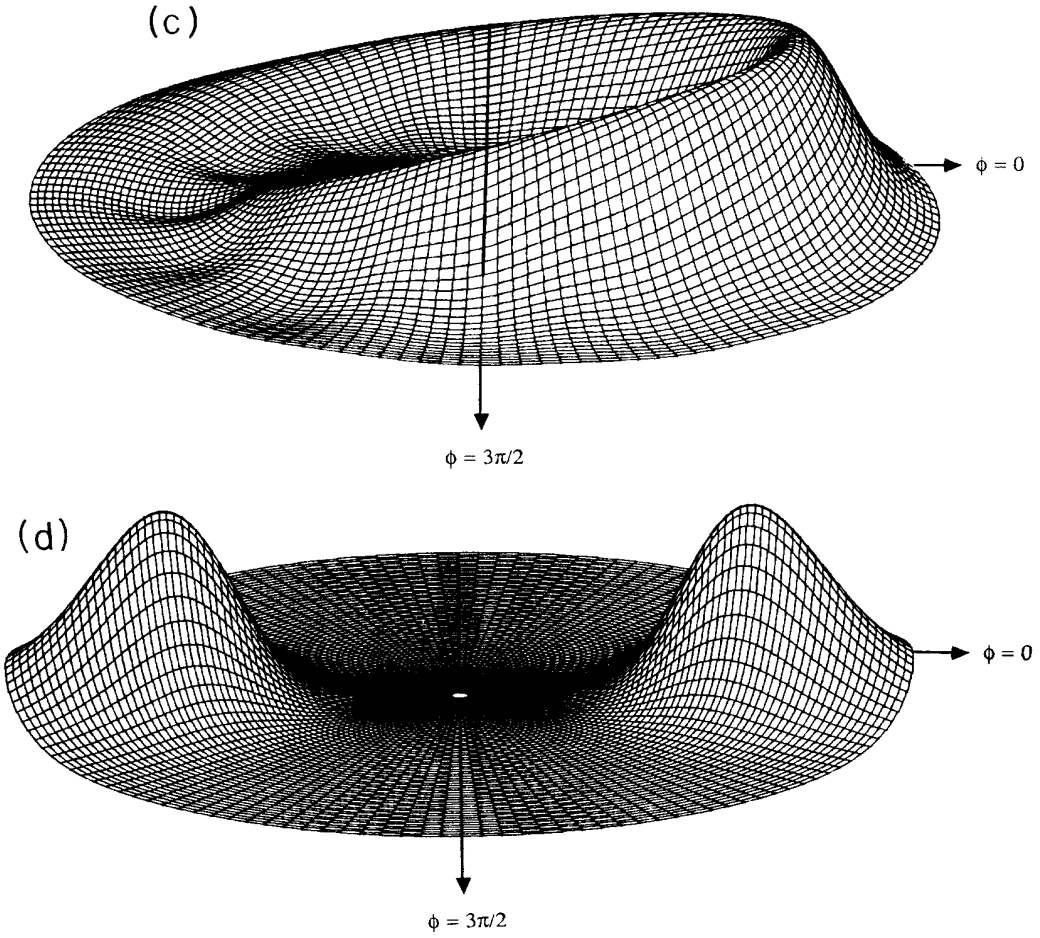

FIG. 1. (*Continued*).

$$Q_j(\gamma;t)=\sum_{n,m=0}^{2j}[S_n^j(\gamma;t)][S_m^j(\gamma;t)]^* \times\exp\left[-\frac{\Gamma t}{2j}(n-m)^2\right] \tag{3.5}$$

for $S_m^j(\gamma;t)$ defined by (2.21) and $Q(\gamma;t)$ reduces to (2.20) for $\Gamma=0$. For $t\gg 2j/\Gamma$, the Q function approaches

$$Q_j(\gamma;t)=[(1+|\gamma_0|^2)(1+|\gamma|^2)]^{-2j} \times\sum_{n=0}^{2j}\binom{2j}{n}^2|\gamma|^{2n}|\gamma_0|^{2n},\quad t\gg 2j/\Gamma \tag{3.6}$$

where phase diffusion has destroyed the phase dependence of Q. The Q function (3.6) is shown in Fig. 4(a) and the phase diffusion of the initial state (2.16), shown in Fig. 1, is evident. Each contour of the Q function is an annulus with the origin at the center $\gamma=0$. In fact, the Q function (3.6) is also the solution to the classical equation of motion,

$$\frac{\partial}{\partial t}Q_j(\gamma;t)=-i\left[\omega+\lambda\frac{1-|\gamma|^2}{1+|\gamma|^2}\right]\gamma\frac{\partial}{\partial\gamma}Q_j(\gamma;t) -\frac{\Gamma}{2j}\left[\gamma\frac{\partial}{\partial\gamma}-\gamma^*\frac{\partial}{\partial\gamma^*}\right]^2Q(\gamma;t) \tag{3.7}$$

for the initial condition (2.16) and $t\gg 2j/\Gamma$. Equation (3.7) describes the evolution of a classical nonlinear rotator given by the Hamiltonian (2.1) with phase diffusion incorporated into the dynamics. Thus, in addition to the semiclassical regime where, for short times, the classical and quantum evolutions of the Q function are similar,

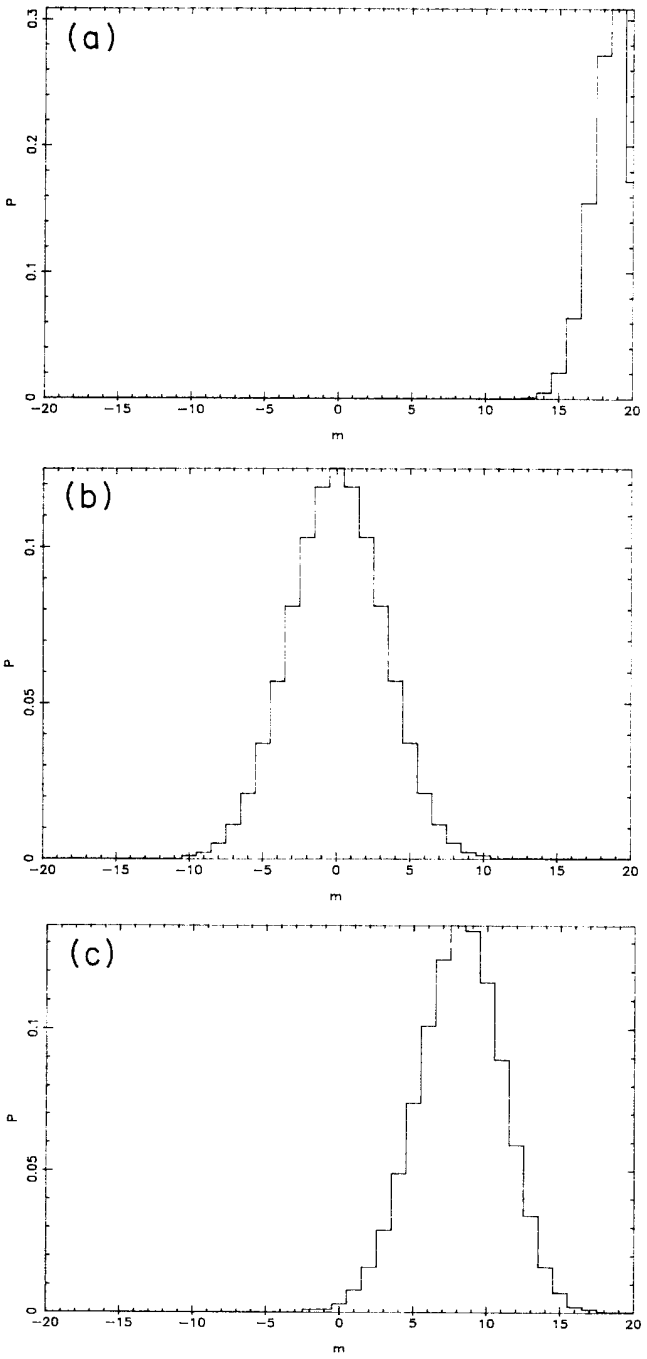

FIG. 2. The (a) J_x, (b) J_y, and (c) J_z eigenvalue distributions for the coherent state $|j=20,\ \gamma_0=0.65\rangle$.

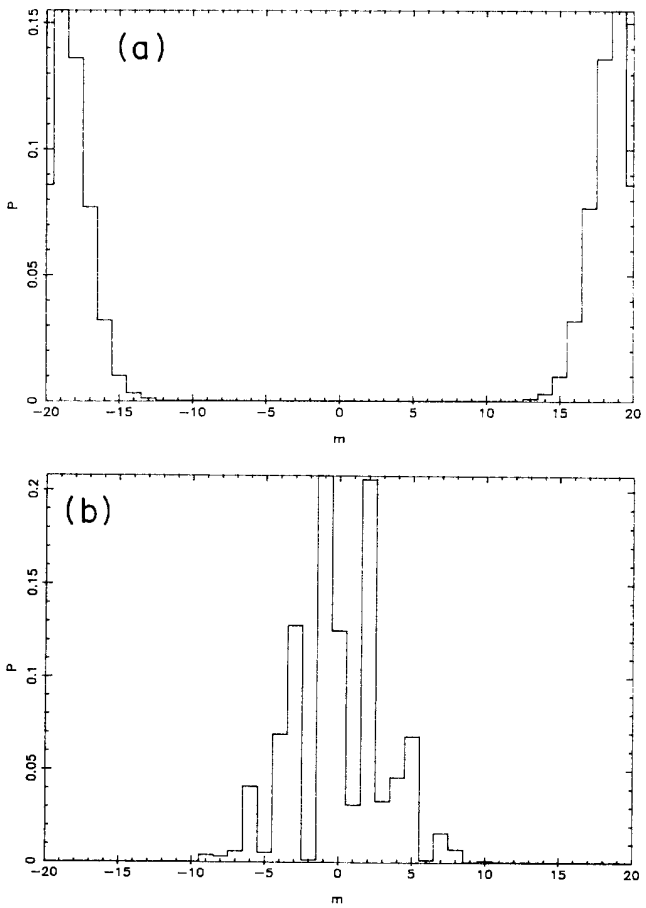

FIG. 3. The (a) J_x and (b) J_y eigenvalue distributions for the $t=20\pi/3$ where $j=20$, $\gamma_0=0.65$, $\omega=0$, and $\lambda=3$.

there exists a long-time semiclassical regime. For j large and $t \gg 2j/\Gamma$, the Q functions for the measured quantum nonlinear rotator and the phase-diffused classical nonlinear rotator converge.

The probability density (3.6) corresponds to the Q function for the state

$$\rho_j = \sum_{m=-j}^{j} |\langle jm|j\gamma_0\rangle|^2 |jm\rangle\langle jm|, \quad t \gg 2j/\Gamma . \tag{3.8}$$

The state (3.7) is a mixture of J_z eigenstates with a distribution of eigenvalues equal to that of the coherent state. Strong measurement has preserved the J_z eigenvalue probability distribution but has destroyed the coherences between the J_z eigenstates. However, the J_x and J_y eigenvalues have been modified by the effect of measurement. In Fig. 4(b) the J_y eigenvalue distribution is shown for $\Gamma t \to \infty$ and is identical to the eigenvalue distribution for the operator $J_x \cos\psi + J_y \sin\psi$ for any ψ. The distribution is bimodal and is symmetric about $m=0$ due to the phase independence of the eigenvalue distribution. A similar bimodal distribution has been observed by Peres[16] for the case of sharp J_z measurements of the state $|j\,j\rangle$ in the J_y eigenbasis.

In Fig. 1(c) ripples present in the Q function provide evidence of coherence effects. In Fig. 5(a), where $\Gamma=1$, $\lambda=3$, and $t=16\pi/15$, the ripples have been suppressed. The introduction of a small measurement parameter has produced a dramatic effect on the coherences observed in the Q function. In Fig. 5(b) we observe that the superposition of two distinct coherent states has partially formed for $t=\tau_j/4$, but the presence of measurement in the dynamics has suppressed the coherences and destroyed the distinctness of the two peaks which appear in the absence of measurement [Fig. 3(b)]. For longer

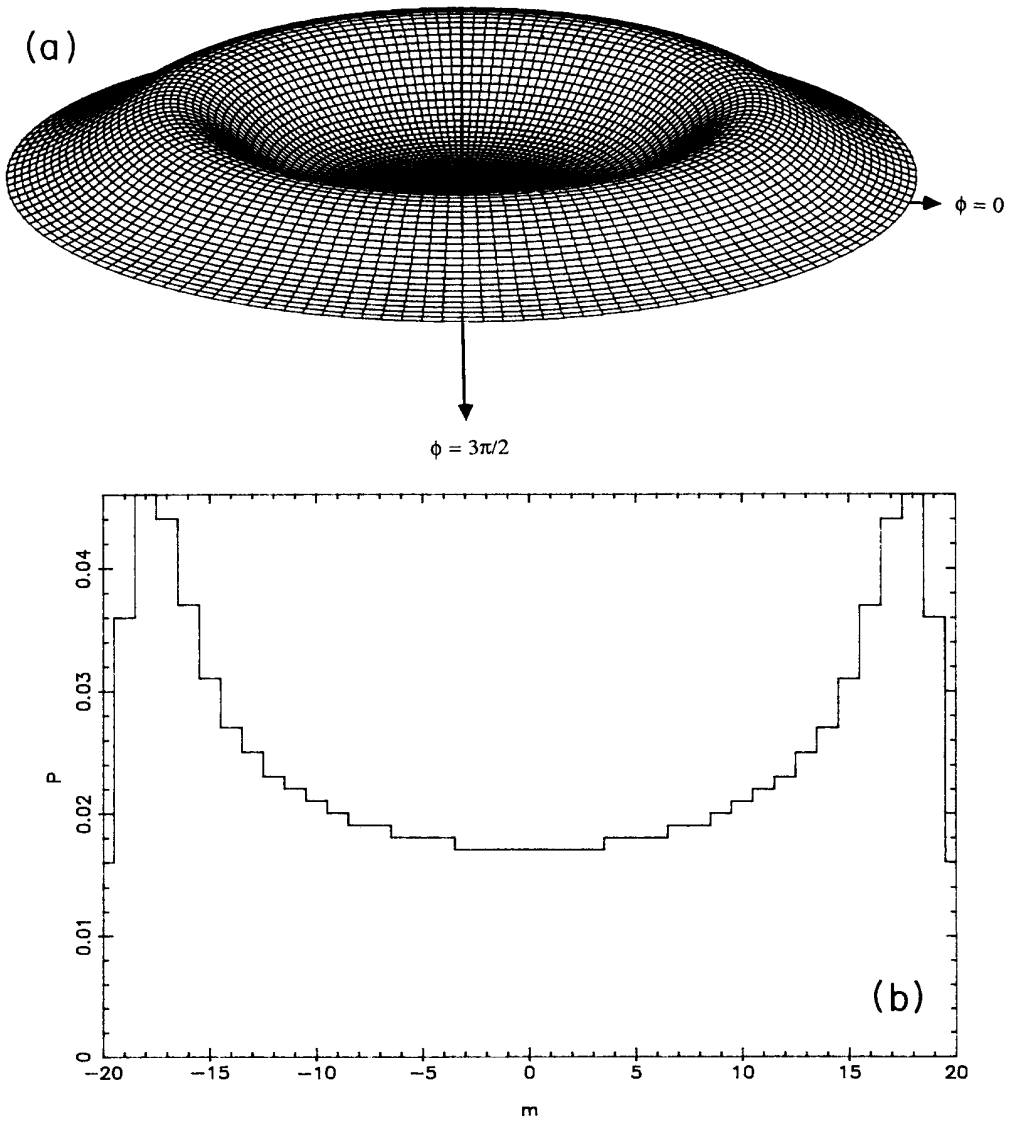

FIG. 4. The (a) quantum probability density $Q(\gamma;t)$, for $|\gamma| \le 1$ and where $Q_{\max}=0.10$, and (b) the J_y eigenvalue distribution for $j=20$, $\gamma_0=0.65$, and $t \gg 2j/\Gamma$.

times the Q function undergoes greater phase diffusion and approaches the state shown in Fig. 4(a). The J_x and J_y eigenvalue distributions also display the effect of measurement. For $\Gamma=1$ and $t=\tau_j/4$ the two peaks in the J_x eigenvalue distribution, shown in Fig. 6(a), are no longer separate, as is the case in Fig. 3(a) for the superposition of two coherent states. In Fig. 6(b) the interference fringes in the J_y eigenvalue distribution are reduced, in contrast to those observed for the superposition state in Fig. 3(b). The J_x and J_y eigenvalue distributions are intermediate between the pure state distributions of Fig. 3 and the mixed-state distribution in Fig. 4(b). The pure state corresponds to $\Gamma=0$. As the ratio Γ/λ increases, the eigenvalue distributions at the time $\tau_j/4$ approaches the mixed-state distribution of Fig. 4(b).

The inverse j scaling of the nonlinear coefficient $\lambda/2j$ and of the measurement coefficient $\Gamma/2j$ and the proportionality of τ_j to j ensure that the degree of quantum coherences and phase diffusion is independent of j for any time $\alpha\tau$ (α is any real number). To illustrate this feature of the model, we compare the eigenvalue distributions for $j=20$ and 40 at the time of the first superposition state $\tau_j/4$. The J_x and J_y eigenvalue distributions for $j=40$, $\gamma_0=0.65$, $\omega=0$, $\lambda=3$, $\Gamma=1$, and $t=\tau_j/4$ are shown in Fig. 7. The delocalization of the two peaks is shown in Fig. 7(a) and the destruction of the interference fringes is shown in Fig. 7(b) for $j=40$. The universal scaling of the degree of quantum coherence and phase diffusion is evident by noting the similarities between Figs. 7 and 6.

IV. A QUANTUM OPTICAL MODEL OF THE NONLINEAR ROTATOR

In principle, a quantum optical model can be constructed to test the quantum nonlinear rotator phenomena described in the preceding sections. If we begin with a two-model field associated with the annihilation operators a and b, then an su(2) algebra can be constructed[17] where

$$J_x=\tfrac{1}{2}(a^\dagger b+ab^\dagger)\ , \tag{4.1a}$$

$$J_y=\frac{1}{2i}(a^\dagger b-ab^\dagger)\ , \tag{4.1b}$$

and

$$J_z=\tfrac{1}{2}(a^\dagger a-b^\dagger b)\ . \tag{4.1c}$$

The Casimir operator is given by

$$\mathbf{J}^2=S(S+1) \tag{4.2a}$$

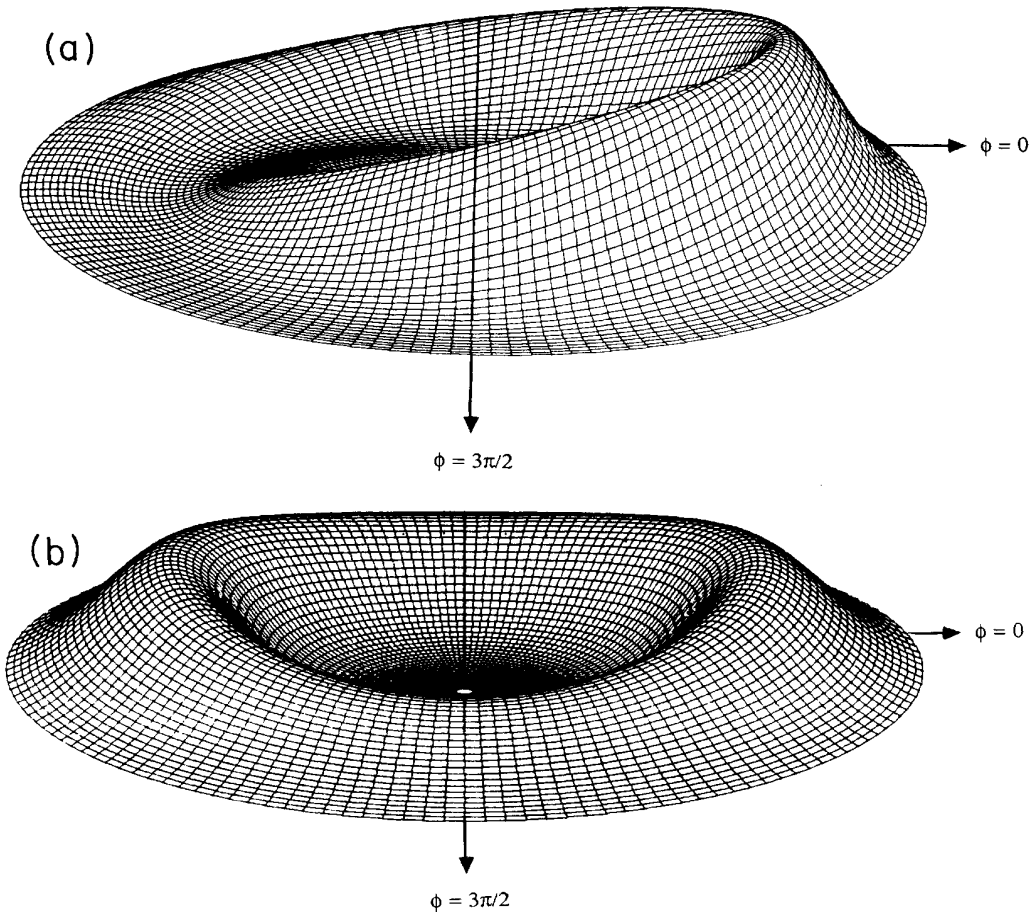

FIG. 5. The quantum probability density $Q(\gamma;t)$, for $r\leq 1$, with $j=20$, $\gamma_0=0.65$, $\omega=0$, $\lambda=3$, and $\Gamma=1$. The densities are shown for (a) $t=16\pi/15$ ($Q_{\max}=0.22$) and (b) $t=20\pi/3$ ($Q_{\max}=0.12$).

for

$$S=\tfrac{1}{2}(a^{\dagger}a+b^{\dagger}b)\ , \tag{4.2b}$$

and S commutes with the operators J_x, J_y, and J_z. In this section we shall prepare an SU(2) coherent state from the two modes. The two modes will then interact in a medium for which the Hamiltonian is given by (2.1) and measurements of J_x, J_y, and J_z are discussed.

The Dicke state $|j\,j\rangle$ is an eigenstate of $\mathbf{J}^2$ and J_z with eigenvalues $j(j+1)$ and j, respectively, where we take j to be a positive integer. The J_z eigenbasis for the Hilbert space is obtained by repeatedly applying the lowering operator $J_-=ab^{\dagger}$ to the state $|j\,j\rangle$. The $2j+1$ J_z eigenstates $|jm\rangle$ can therefore be expressed in the a and b modes as[17]

$$|jm\rangle=|2j-m\rangle_a\otimes|m\rangle_b\ . \tag{4.3}$$

Therefore, the Dicke state $|jm\rangle$ corresponds to the a mode in the Fock number state $|2j-m\rangle_a$ and the b mode in the state $|m\rangle_b$. The preparation of the Fock states of the electromagnetic field requires the use of selective measurements. Examples of Fock-state generation schemes include the micromaser[18] and the parametric amplifier.[19] We assume that photon detectors with unit efficiency are used to generate SU(2) coherent-coherent states: the effects of nonunit quantum efficiency in the photon detectors on the SU(2) coherent states require further investigation.

The SU(2) coherent state $|j\gamma\rangle$ is obtained by applying the rotation operator (2.6a) to the state $|j\,j\rangle$, as shown in Eq. (2.6c). In the a and b modes, the rotation operator is given by

$$R(\gamma)=\exp[\tfrac{1}{2}\theta(e^{i\varphi}ab^{\dagger}-e^{-i\varphi}a^{\dagger}b)] \tag{4.4}$$

for γ given by (2.3). The interaction necessary to generate the rotation (4.4) involves using a $\chi^{(2)}$ medium as a parametric frequency converter. The pump field is treated classically and θ is proportional to the pump-field strength, the nonlinearity, and the length of the $\chi^{(2)}$ medium. The phase parameter φ is controlled by passing the pump field through a phase shifter prior to the frequency converter interaction. The SU(2) coherent state is therefore obtained by injecting the state $|2j\rangle_a\otimes|0\rangle_b$ into the frequency converter where the pump-field strength and the phase are chosen to select the appropriate state.

The existence of a coherent state can be verified by

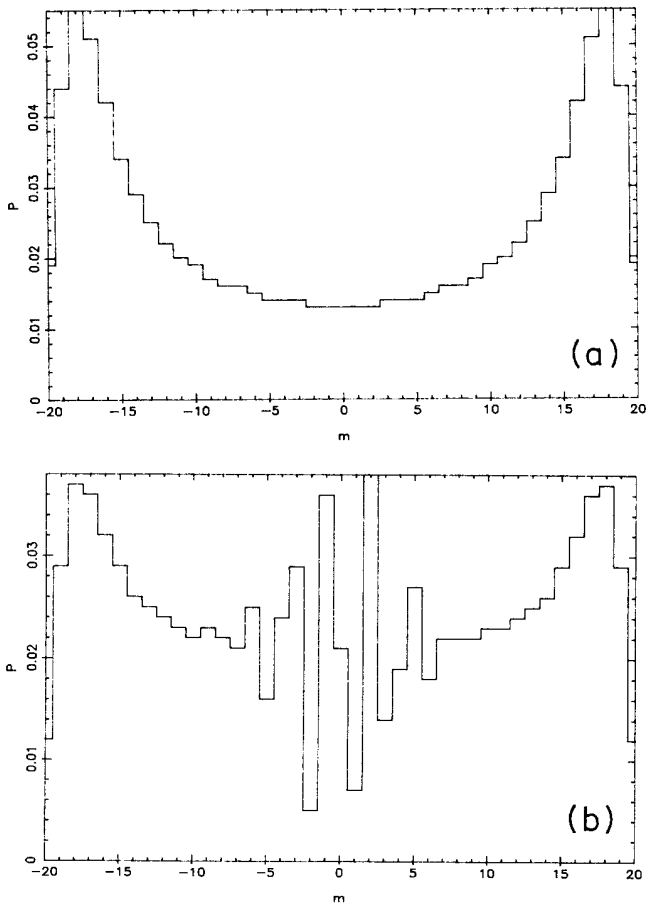

FIG. 6. The (a) J_x and (b) J_y eigenvalue distributions for the measured rotator where $j=20$, $\gamma_0=0.65$, $\omega=0$, $\lambda=3$, $\Gamma=1$, and $t=20\pi/3$.

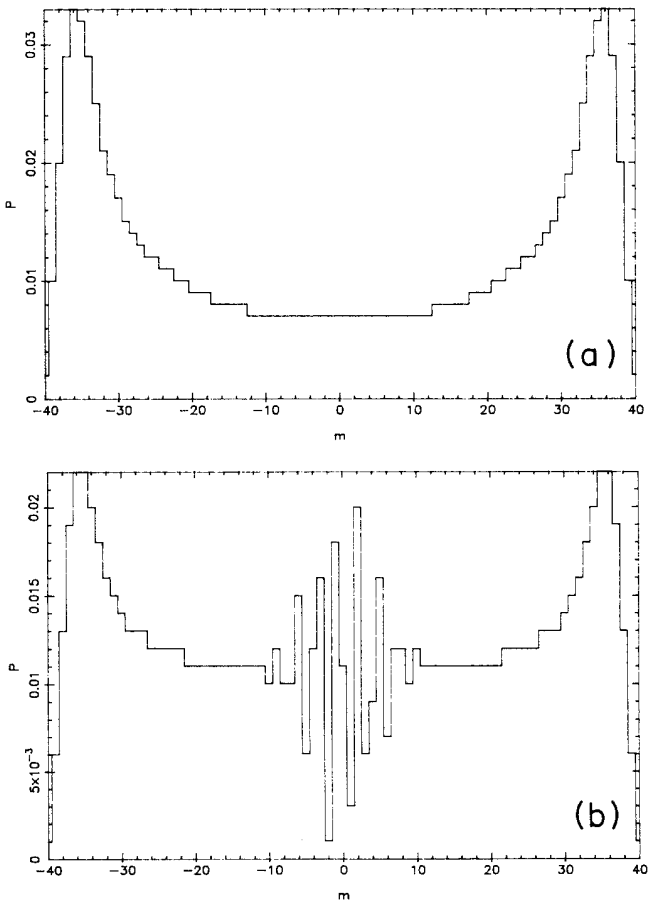

FIG. 7. The (a) J_x and (b) J_y eigenvalue distributions for the measured rotator where $j=40$, $\gamma_0=0.65$, $\omega=0$, $\lambda=3$, $\Gamma=1$, and $t=40\pi/3$.

measuring J_x, J_y, and J_z. The distribution of readings of the J_x, J_y, and J_z operators should correspond to those of the coherent state, as shown, for example, in Fig. 4. Here we establish physical measurements of the J_i quantities. To measure J_x and J_y, an apparatus similar to that of a balanced quantum homodyne detector is used[20] and is described below. The a mode can be identified with the signal field and mode b with the local oscillator.

The b mode encounters a phase shifter which induces a phase shift of ψ on the b field. The a mode and the phase-shifted b mode are then obtained by a $\frac{50}{50}$ beam splitter and the output fields are given by

$$c=2^{-1/2}(1+ibe^{i\psi}),\quad d=2^{-1/2}(be^{i\psi}+ia)\ . \tag{4.5}$$

A photon counter is placed at each of the two beam-splitter output ports and the half-difference of photon counts from the two ports is measured. Thus, the measured quantity corresponds to the operator

$$\begin{aligned}\tfrac{1}{2}(d^\dagger d-c^\dagger c)&=\tfrac{1}{2}i(ab^\dagger e^{-i\psi}-a^\dagger be^{i\psi})\\&=J_x\sin\psi+J_y\cos\psi\ .\end{aligned} \tag{4.6}$$

Thus a beam splitter to combine the a and b modes followed by a photon-count difference measurement allows the direct measurement of any combination of J_x and J_y depending on the b-mode phase-shift parameter ψ.

A measurement of J_z is very straightforward. The a and b modes are not combined by a beam splitter. Instead, a photon-counter measures the quanta in each mode and the half-difference of quanta is recorded. In this way measurements of J_z are performed as J_z corresponds to the operator $\frac{1}{2}(a^\dagger a-b^\dagger b)$. The statistics for ideal measurements of J_x, J_y, and J_z conform to the eigenvalue distributions of the angular-momentum components for the SU(2) coherent state. A measurement of $\mathbf{J}^2$ can be obtained by measuring the average photon number in the two modes given by the quantity S defined in (4.2b).

We have established the procedure for generating an SU(2) coherent state by subjecting an a-mode even-number state and the b-mode vacuum state to a $\chi^{(2)}$ interaction. The pump-field phase and intensity are selected to produce the desired coherent state. We have also established the method for producing ideal measurements of J_x, J_y, and J_z in this quantum optical model. Now we require a method for generating the nonlinear Hamiltonian (2.1).

In a $\chi^{(3)}$ medium the Hamiltonian which describes the dynamics is given by[21,22]

$$\begin{aligned}H/\hbar=&\omega_a a^\dagger a+\omega_b b^\dagger b+2\chi_{ab}a^\dagger ab^\dagger b+\tfrac{1}{2}\chi_a(a^\dagger a)^2\\&+\tfrac{1}{2}\chi_b(b^\dagger b)^2\ ,\end{aligned} \tag{4.7}$$

where the nonlinear coefficients χ_i are the components of the $\chi^{(3)}$ tensor for the medium. In practice, the constraint $\chi\equiv\chi_a=\chi_{ab}=\chi_b$ is generally true. We let the a and b modes then pass and interact in the medium for a time T. Let us then pass the a and b modes through two separable Kerr media where the a and b modes do not interact.[22] In these two sections of Kerr medium a and b undergo nonlinear self-phase shifts but interaction between the a and b modes does not occur. The duration for these interactions is t. Thus the unitary evolution operator for the system is given by

$$\begin{aligned}U=\exp\{&-i(\omega_a a^\dagger a+\omega_b b^\dagger b)(T+t)\\&-\tfrac{1}{2}i\chi[(a^\dagger a)^2+(b^\dagger b)^2](T+t)\\&-2i\chi a^\dagger ab^\dagger bT\}\ .\end{aligned} \tag{4.8}$$

Let us define the constants

$$\alpha\equiv(\omega_a+\omega_b)(T+t)\ , \tag{4.9a}$$

$$\omega\equiv(\omega_a-\omega_b)(T+t)\ , \tag{4.9b}$$

$$\beta\equiv\chi(t+3T)\ , \tag{4.9c}$$

and

$$\lambda=2j\chi(t-T)\ , \tag{4.9d}$$

where j is given by the constant of motion $S=\frac{1}{2}(a^\dagger a+b^\dagger b)=j$. Hence the unitary evolution operator (4.8) can be expressed in the angular momentum algebra as

$$\begin{aligned}U&=\exp\left[-i\left[\alpha S+\beta S^2+\omega J_z+\frac{\lambda}{2j}J_z^2\right]\right]\\&=\exp[-i(\alpha j+\beta j^2)]\exp\left[-i\left[\omega J_z+\frac{\lambda}{2j}J_z^2\right]\right]\ .\end{aligned} \tag{4.10}$$

The unitary evolution operator (4.10) corresponds to the evolution operator for the nonlinear rotator Hamiltonian (2.1) for a unit time interval and there is an unimportant j-dependent phase factor. Thus a careful choice of Kerr medium interaction times T and t allows for the construction of the nonlinear rotator evolution.

To summarize this section, a quantum optical model of the nonlinear rotator is prepared as follows. The Dicke $|j\,j\rangle$ state corresponds to the two-mode field state, where one mode is in the number state with $2j$ photons and the other mode is in the vacuum state. An SU(2) coherent state is generated by a $\chi^{(2)}$ frequency converter and the pump-field intensity and phase are adjusted to obtain the desired SU(2) coherent state. The nonlinear rotator interaction is obtained by first causing the two modes to interact in a nonlinear Kerr medium and then subjecting the two modes to two separate Kerr media, in which the two modes undergo a nonlinear self-phase shift but do not interact with each other. To measure J_x and J_y, one mode passes through an adjustable phase shifter and the two modes are combined at a beam splitter. The difference between the quanta emitted at the two beam-splitter output ports corresponds to a measurement of J_x or J_y depending on the phase-shifter parameter. A J_z measurement corresponds to simply counting the difference of quanta in the two modes, a and b.

There are several difficulties with realizing a quantum optical model for the nonlinear rotator. First, the preparation of an SU(2) coherent state requires selective measurement techniques, with very efficient photon detectors. Second, the generation of superposition states

would be degraded by losses in the Kerr medium which destroy the necessary quantum coherences. Furthermore measurements of J_x, J_y, and J_z are degraded by imperfect photon-counting measurements. However, we are currently investigating the effects of losses and imperfect photon-counting devices on the dynamics. It is our hope that the model presented here will allow for the experimental generation of SU(2) coherent states and of superpositions of distinct SU(2) coherent states.

ACKNOWLEDGMENTS

I would like to thank Dr. G. J. Milburn for many valuable discussions. This work has been supported by the Australian Research Council.

[1]G. J. Milburn, Phys. Rev. A **33**, 674 (1986).
[2]G. J. Milburn and C. A. Holmes, Phys. Rev. Lett. **56**, 2237 (1986).
[3]D. J. Daniel and G. J. Milburn, Phys. Rev. A **39**, 4628 (1989).
[4]B. Yurke and D. Stoler, Phys. Rev. Lett. **57**, 13 (1986).
[5]M. Kitigawa and Y. Yamamoto, Phys. Rev. A **34**, 3974 (1986).
[6]P. Tombesi and A. Mecozzi, J. Opt. Soc. Am. B **4**, 1700 (1987).
[7]B. C. Sanders, Phys. Rev. A **39**, 4284 (1989).
[8]M. V. Berry and J. Goldberg, Nonlinearity **1**, 1 (1988).
[9]C. L. Mehta and E. C. G. Sudarshan, Phys. Rev. **138B**, 274 (1965).
[10]A. Perelomov, *Generalized Coherent States and Their Applications* (Springer-Verlag, Berlin, 1986); F. T. Arrechi, E. Courtens, R. Gilmore, and H. Thomas, Phys. Rev. A **6**, 2211 (1972).
[11]A. Barchielli, Phys. Rev. D **32**, 347 (1985).
[12]C. M. Caves and G. J. Milburn, Phys. Rev. A **36**, 5543 (1987).
[13]G. J. Milburn, J. Opt. Soc. Am. B **5**, 1317 (1988).
[14]B. C. Sanders and G. J. Milburn Z. Phys. B (to be published).
[15]F. Haake, M. Kuś, and R. Scharf, Z. Phys. B **65**, 381 (1987).
[16]A. Peres, Phys. Rev. D **39**, 2943 (1989).
[17]B. G. Wybourne, *Classical Groups for Physicists* (Wiley, New York, 1974).
[18]P. Filipowicz, J. Javanainen, and P. Meystre, J. Opt. Soc. Am. B **3**, 906 (1986); P. Meystre and J. J. Slosser, Opt. Commun. **70**, 103 (1989); J. Krause, M. O. Scully, T. Walther, and H. Walther, Phys. Rev. A **39**, 1915 (1989).
[19]G. J. Milburn, C. A. Holmes, and D. F. Walls Phys. Rev. A **39**, 2493 (1989).
[20]H. P. Yuen and J. H. Shapiro, in *Coherence and Quantum Optics IV*, edited by L. Mandel and E. Wolf (Plenum, New York, 1980).
[21]P. Alsing, G. J. Milburn, and D. F. Walls, Phys. Rev. A **37**, 2970 (1988).
[22]B. C. Sanders and G. J. Milburn, Phys. Rev. A **39**, 694 (1989).